Structure elucidation and characterization of patulin synthase, insights into the formation of a fungal mycotoxin

Tjallinks, Gwen; Boverio, Alessandro; Maric, Ivana; Rozeboom, Henriette; Arentshorst, Mark; Visser, Jaap; Ram, Arthur F J; Mattevi, Andrea; Fraaije, Marco W

IMPORTANT NOTE: You are advised to consult the publisher's version (publisher's PDF) if you wish to cite from it. Please check the document version below.

Document Version
Publisher's PDF, also known as Version of record

Publication date:
2023

Link to publication in University of Groningen/UMCG research database

Citation for published version (APA):
Tjallinks, G., Boverio, A., Maric, I., Rozeboom, H., Arentshorst, M., Visser, J., Ram, A. F. J., Mattevi, A., & Fraaije, M. W. (2023). Structure elucidation and characterization of patulin synthase, insights into the formation of a fungal mycotoxin. *The FEBS Journal*, *290*(21), 5114-5126. Article 16804. https://doi.org/10.1111/febs.16804

Structure elucidation and characterization of patulin synthase, insights into the formation of a fungal mycotoxin

Gwen Tjallinks[1,2], Alessandro Boverio[1,2], Ivana Maric[1], Henriette Rozeboom[1], Mark Arentshorst[3], Jaap Visser[3], Arthur F. J. Ram[3] (iD), Andrea Mattevi[2] (iD) and Marco W. Fraaije[1] (iD)

1 Molecular Enzymology, University of Groningen, The Netherlands
2 Department of Biology and Biotechnology, University of Pavia, Italy
3 Institute of Biology Leiden, Leiden University, The Netherlands

Patulin synthase (PatE) from *Penicillium expansum* is a flavin-dependent enzyme that catalyses the last step in the biosynthesis of the mycotoxin patulin. This secondary metabolite is often present in fruit and fruit-derived products, causing postharvest losses. The *patE* gene was expressed in *Aspergillus niger* allowing purification and characterization of PatE. This confirmed that PatE is active not only on the proposed patulin precursor ascladiol but also on several aromatic alcohols including 5-hydroxymethylfurfural. By elucidating its crystal structure, details on its catalytic mechanism were revealed. Several aspects of the active site architecture are reminiscent of that of fungal aryl-alcohol oxidases. Yet, PatE is most efficient with ascladiol as substrate confirming its dedicated role in biosynthesis of patulin.

Introduction

Penicillium expansum is a widespread blue mould frequently found in the environment [1,2]. While it is a common fungus in soil and air, it is also one of the most important pathogens in a wide range of agricultural products [3]. Especially fruits, such as apples and pears, are primary targets for this toxigenic fungus [4]. Once it has infected the host, *P. expansum* produces a range of secondary metabolites as virulence factors and one of the most studied and notorious metabolites is patulin. Patulin is a mycotoxin with strong antibiotic activity towards a range of bacteria and fungi, which aids the competitiveness of *P. expansum* [5]. Moreover, patulin is carcinogenic towards mammals and its levels in food products are therefore bound to regulations prescribed by organizations such as the US

Food and Drug Administration and the World Health Organization [6,7]. As a result, patulin is one of the major factors for postharvest losses of fruit and vegetables [8,9].

Patulin is produced through a biosynthetic gene cluster consisting of a variety of different enzymes. This polyketide pathway has been identified in various fungal genera such as *Aspergillus* [10], *Byssochlamys* [11], *Paecilomyces* [12,13] and *Penicillium* [14]. However, the major contributor to patulin contamination of fruits and vegetables is *P. expansum* [8]. The biochemical pathway consists of 10 enzymatic reactions starting from acetate [4]. Several essential enzymes in the biosynthesis of patulin have been characterized, including PatK which catalyses the first step in the

Abbreviations

AAO, aryl-alcohol oxidase; DFF, 2,5-diformylfuran; EndoH, Endoglycosidase H; FAD, flavin adenine dinucleotide; FDCA, 2,5-furandicarboxylic acid; FFCA, 5-formyl-2-furancarboxylic acid; GMC, glucose-methanol-choline; HMF, 5-hydroxymethyl furfural; HPLC, high-performance liquid chromatography; PatE, patulin synthase; RMSD, root mean square deviation.

reaction, PatG that converts 6-methylsalicylic acid to *m*-cresol, and PatH and PatI which are both cytochrome P450 monooxygenases leading to the formation of gentisyl alcohol (Fig. 1). Nevertheless, the enzyme required for the last step and actual synthesis of the toxin patulin, named patulin synthase, has not yet been biochemically characterized. It has been suggested that patulin synthase performs a primary alcohol oxidation of the substrate ascladiol to the corresponding aldehyde, triggering a spontaneous ring closure to form the hemiacetal patulin.

Patulin synthase (PatE) is encoded for by the gene *patE* and belongs to the glucose-methanol-choline (GMC) oxidoreductase family. GMC oxidoreductases typically contain flavin adenine dinucleotide (FAD) as tightly bound organic cofactor and often use molecular oxygen as electron acceptor [15]. GMC oxidases are composed of two domains; an N-terminal conserved FAD domain and a C-terminal nonconserved substrate domain [16]. Members of this enzyme class of enzymes have been shown to act on widely differing compounds, being involved in various processes such as

lignocellulose degradation to mycotoxin formation [17–19]. Here, a detailed structural and biochemical analysis of PatE was performed to shed light on its catalytic and structural properties.

Results and discussion

Characteristics and stability

We tested various expression vectors (pBAD- and pET-based), *Escherichia coli* strains, expression conditions and fusion protein expression constructs to express PatE. Yet, no expression of soluble protein could be obtained. As alternative for expressing this fungal flavoprotein, expression in *Aspergillus niger* was explored using a newly developed CRISPR/Cas9-based approach. Gratifyingly, patulin synthase with a C-terminal His-tag was successfully obtained via heterologous extracellular expression in *A. niger* [20]. In fact, PatE was the most dominant secreted protein present in the medium (Fig. 2A). Immobilized metal ion affinity chromatography was performed to obtain a highly pure
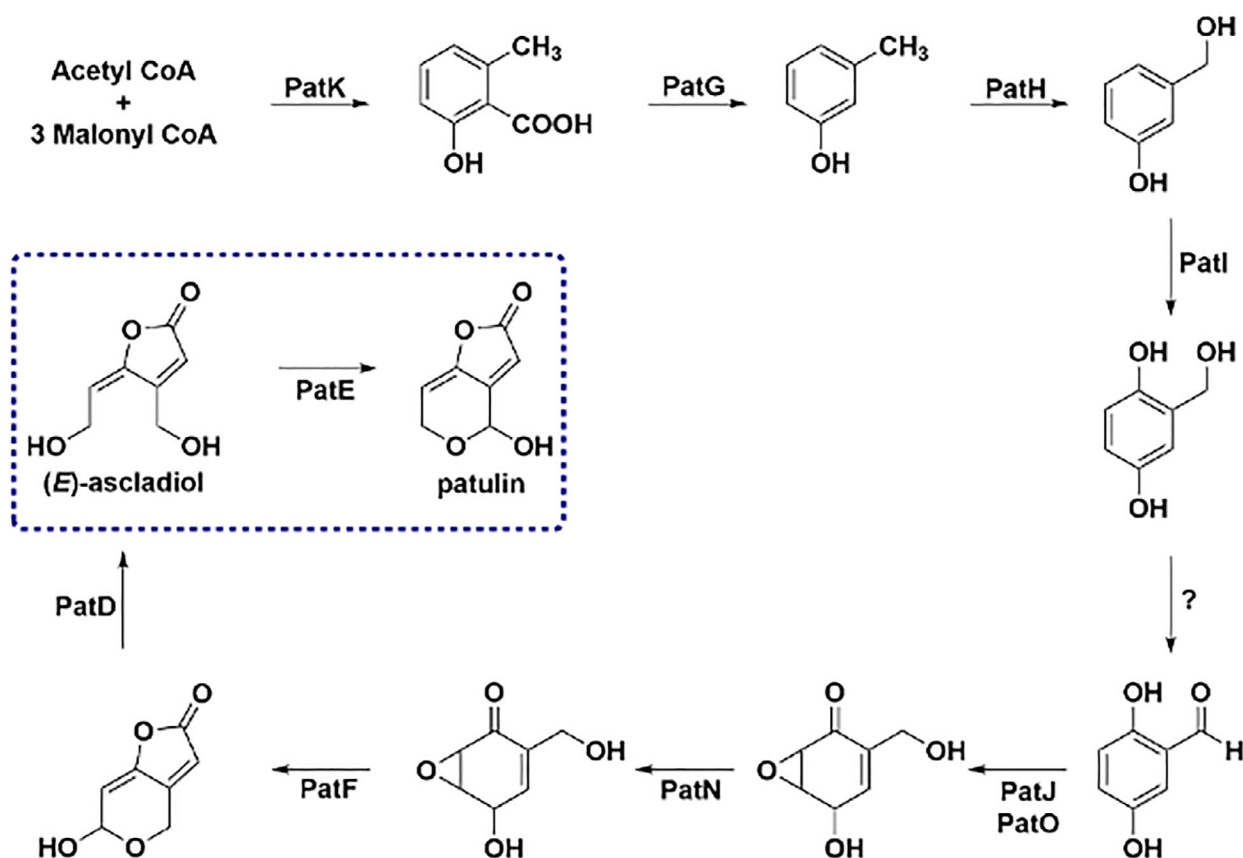

Fig. 1. Overview of the biosynthetic pathway towards the production of patulin. The oxidation of (*E*)-ascladiol by patulin synthase has been highlighted by a box.
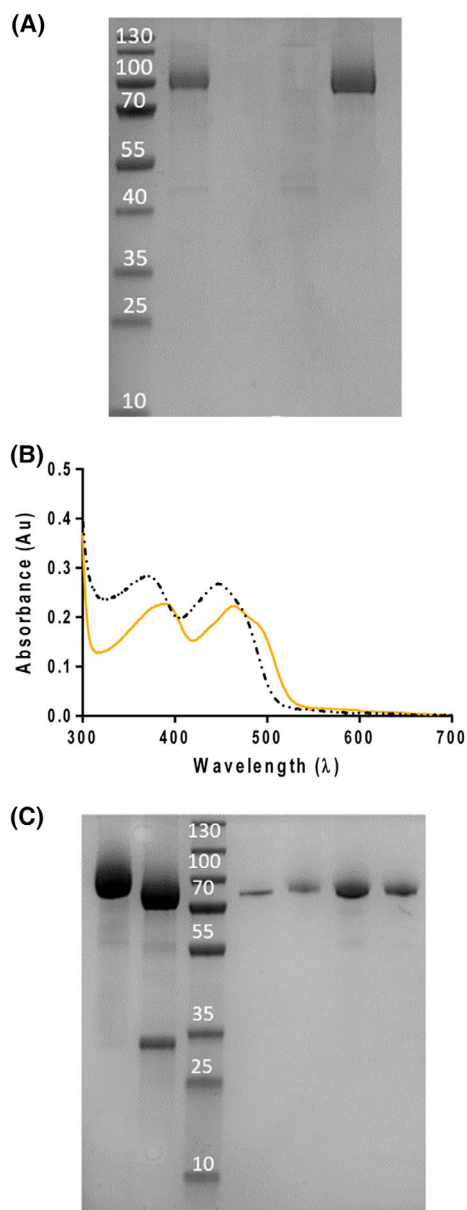
(A)

(B)

(C)

Fig. 2. (A) SDS/PAGE gel purification of PatE. From left to right: marker, supernatant, flow-through, wash and elute. (B) UV–Vis absorbance spectrum of pure (yellow line) and denatured (dotted line) PatE to calculate the extinction coefficient. (C) SDS/PAGE gel of deglycosylation and gel filtration of PatE. From left to right: glycosylated PatE, deglycosylated PatE with EndoH, marker, pooled fractions after size-exclusion chromatography.

and yellow-coloured protein fraction (Fig. 2A). The purified enzyme shows a characteristic flavin spectrum, having absorbance maxima around 391 and 463 nm (Fig. 2B). Patulin synthase has seven predicted *N*-glycosylation sites, resulting in an expected molecular weight of 85.6 kDa (if estimating an extra 2.5 kDa per *N*-glycosylation site). SDS/PAGE revealed a protein

band corresponding to a molecular weight of around 95 kDa, which is in the range of the expected molecular weight. SDS/PAGE analysis of Endoglycosidase H (EndoH)-deglycosylated protein resulted in a clear shift of the protein band by about 10 kDa (Fig. 2C). The molecular weight of the deglycosylated protein comes close to the expected molecular weight of secreted His-tagged PatE (67.1 kDa). The apparent higher molecular weight can be partly due to the remaining *N*-acetylglucosamine moieties upon EndoH digestion, partial deglycosylation and/or partial removal of the secretion signal peptide. It is worth noting that the enzyme was obtained in high purity, displaying a sharp protein band upon SDS/PAGE (Fig. 2C).

Next, the thermostability of patulin synthase at pH 7.5 before and after EndoH treatment was measured using the *Thermo*FAD method. While significant glycosylation was confirmed by SDS/PAGE analysis, no significant difference in thermostability was observed with apparent melting temperatures of 45 °C for both enzyme preparations (Fig. 3A). Except for the protein crystallization experiments, all biochemical characterization experiments were performed using the glycosylated patulin synthase. The thermostability of patulin synthase was examined using various buffers covering a broad pH range (pH 5–9). The enzyme was shown to be most stable at low pH values (Fig. 3B). Since many fungi prefer acidic growth conditions, it is not surprising that the highest enzyme stability was found at the lowest pH tested (pH 5).

Substrate screening and steady-state kinetics

Next, it was tested whether, as postulated, PatE is in fact an oxidase acting on ascladiol. For this, the HRP-coupled oxidase assay was used, which indeed confirmed that PatE can act as an ascladiol oxidase. GMC-type oxidases often display a broad substrate specificity [17,19]. To investigate the substrate scope of PatE, 60 additional potential substrates ranging from carbohydrates to aliphatic and aromatic alcohols were probed for oxidase activity using the HRP-based assay (Table S1). With 1.0 μM of patulin synthase and 10 mM of each test substrate, it was quickly observed that PatE exclusively accepts aromatic alcohols as substrate. Of the 12 tested aromatic alcohols, nine were found to be a substrate. All other tested alcohols did not show any activity. One evident example is the activity detected towards 1,2-benzenedimethanol where patulin synthase did not display activity towards the nonaromatic equivalent cyclohexane-1,2-diyldimethanol. For all identified substrates, the steady-state kinetic parameters were determined (Table 1, Fig. 4).
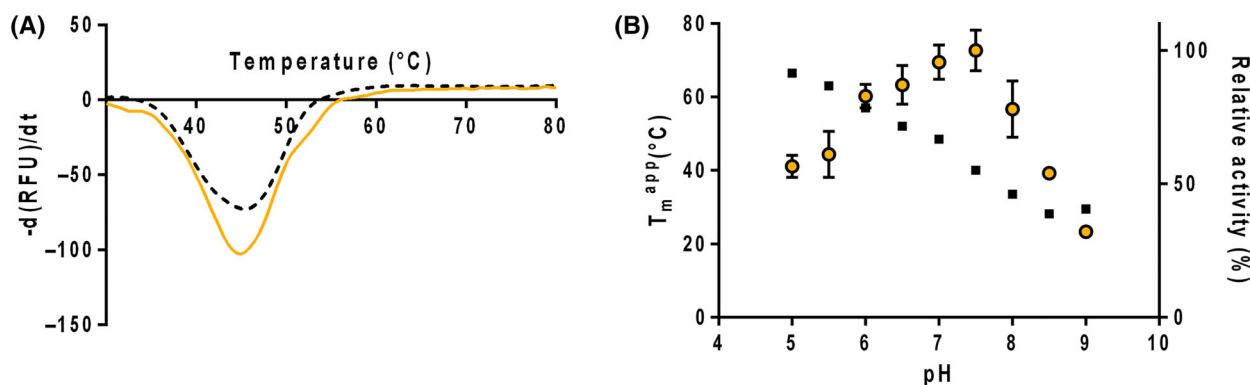
Fig. 3. (A) Melting temperature of glycosylated (yellow line) and deglycosylated (dotted line) PatE in 100 mM KPi pH 7.5 with the thermoFAD methodology. (B) PatE activity (○) and stability (■) is pH-dependent. For thermostability measurements, 20 μM PatE was used, while activity was measured using 1.0 μM PatE and 10 mM 3-methoxybenzyl alcohol. Both experiments were performed in triplicate (*n* = 3).

Upon determining the steady-state kinetic parameters, it became clear that the natural substrate ascladiol is the preferred substrate as it displays the lowest K_M towards the patulin precursor. Only one identified substrate, benzyl alcohol, displayed a slightly higher k_{cat} when compared with ascladiol (15.7 vs. 11.5 s^{-1}). Yet, it displays a > 40-fold higher K_M value for benzyl alcohol. Interestingly, the enzyme also suffers from severe substrate inhibition with ascladiol as substrate. This may serve as a feedback mechanism preventing too much patulin build-up in the environment. Except for 4-methoxybenzyl alcohol, all other six-membered aromatic alcohols did not exhibit significant substrate inhibition. Perchance, due to the larger size of these substrates, they cannot form strong binding interactions with the enzyme-substrate complex, which in turn would prevent inhibition from taking place.

Since the pH profile for enzyme stability does not have to correlate with that of enzyme activity, oxidase activity was measured at different pH values. This

showed that PatE displays highest activity at pH 7.5 (Fig. 3B). The activity profile shows a drastic decline in activity at higher pH values. At pH values below pH 7.5, the activity decrease was more gradual. This might be due to the pK_a of the catalytic-base histidine in the active site, which is approximately 6 and therefore protonated below that pH. Hence, activity increases when the pH is above 6. The more drastic decline in activity at high pH values may be due to protein unfolding events, which is in line with the thermostability measurements.

Using HPLC analysis, we could monitor ascladiol consumption and patulin production over time. After 1 h, 50% of ascladiol was converted by PatE and a new peak appeared corresponding to patulin (Fig. 5). Furthermore, an additional peak showed up at a lower retention time, which is probably the aldehyde derivative of ascladiol, before ring closure occurs. This aldehyde intermediate disappeared over time but did not lead to an increase in patulin in the reaction mixture

Table 1. Steady-state kinetic parameters for patulin synthase[a].

Substrate	k_{cat} (s^{-1})	K_M (mM)	k_{cat}/K_M (s^{-1}·M^{-1})	K_I (mM)
Ascladiol	11.5 ± 1.8	0.9 ± 0.2	12.8 × 10^3	4.3
3-Methoxybenzyl alcohol	2.2 ± 0.06	3.3 ± 0.3	667	n.d.[b]
Benzyl alcohol	15.7 ± 1.9	41.4 ± 11.7	379	n.d.
1,2-Dimethanolbenzene	3.7 ± 0.1	10.1 ± 1.1	366	n.d.
5-Hydroxymethyl furfural	0.4 ± 0.04	4.7 ± 1.0	85	28
Furfuryl alcohol	0.5 ± 0.1	12.1 ± 4.5	41	43
4-Methoxybenzyl alcohol	0.16 ± 0.07	11.3 ± 1.9	14	11
Vanillyl alcohol	0.64 ± 0.03	52.3 ± 5.8	12	n.d.
2,5-Dimethanolfuran	0.1 ± 0.008	24.7 ± 2.6	4.0	58
3,4-Methoxybenzyl alcohol	0.23 ± 0.03	73.9 ± 16.6	3.1	n.d.

[a]Values obtained at 25 °C using 100 mM KPi buffer pH 7.5.; [b]The term n.d. stands for not determined, since no substrate inhibition was observed.
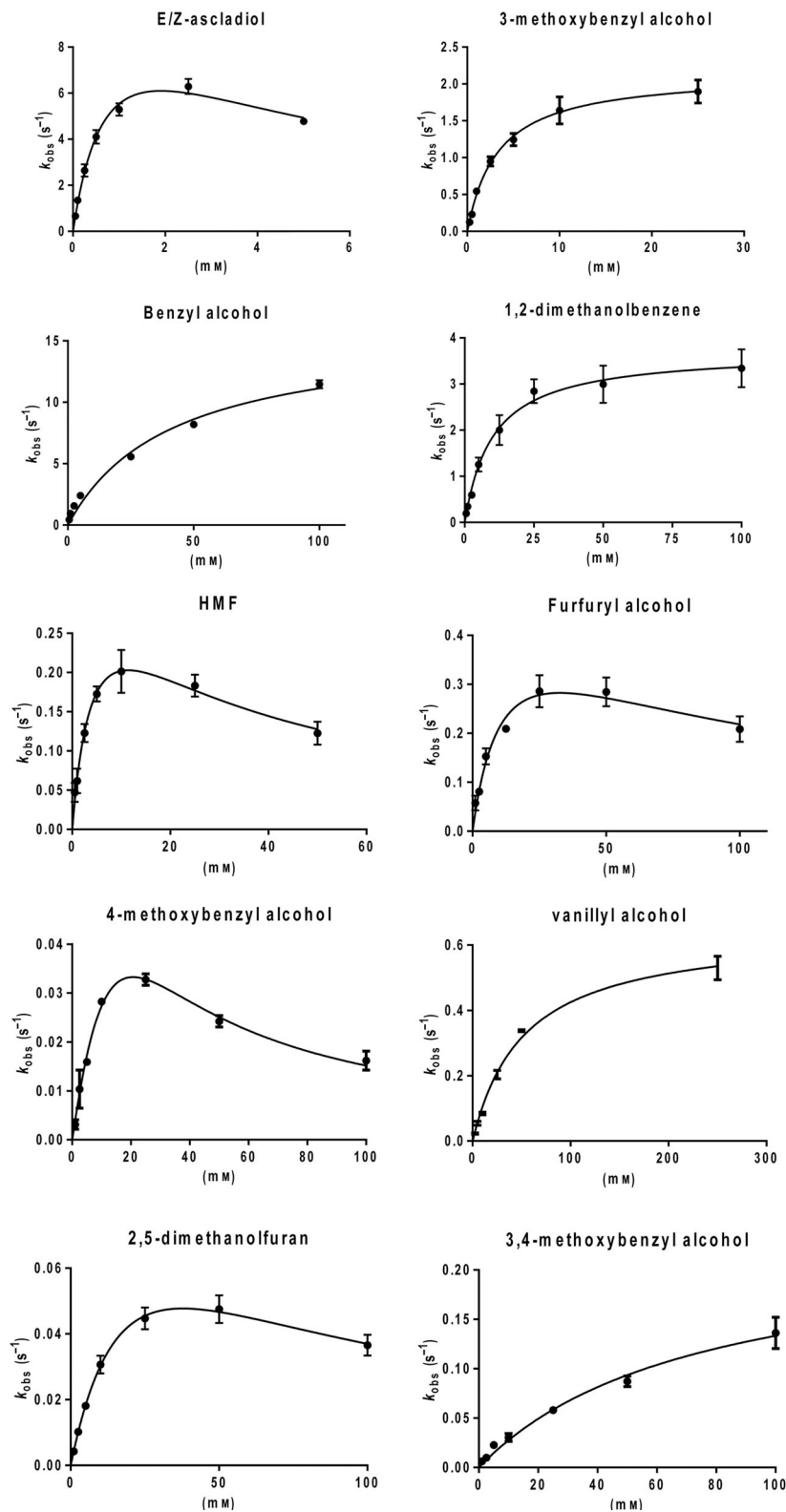
Fig. 4. Michaelis–Menten fit of the values obtained testing PatE with different aromatic alcohols. All points were taken in triplicates ($n = 3$).
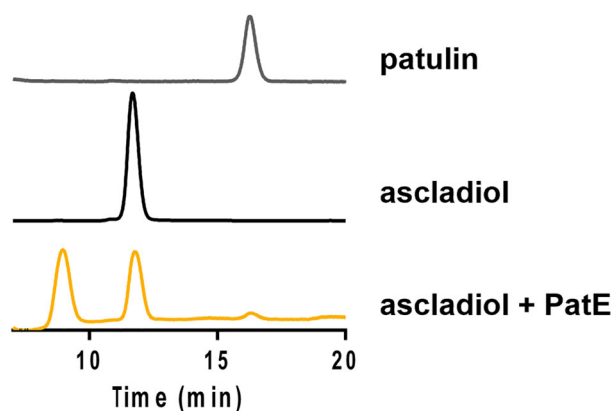
Fig. 5. HPLC analysis of ascladiol conversion by PatE. Top chromatograms are elution patterns for patulin and ascladiol, respectively. The lower chromatogram was obtained after 1 h aerobic incubation of 0.5 mM ascladiol with 0.1 μM PatE.

(Fig. S1). It is known that ascladiol is relatively unstable; hence, the aldehyde derivative could convert in a mixture of unidentified products [21]. Furthermore, importantly, only the (*E*)-enantiomer of ascladiol can lead to ring closure. However, the chemically synthesized ascladiol used was predominantly in the (*Z*)-configuration due to its higher thermodynamic stability. Hence, it is likely that predominantly the (*Z*)-isomer of the aldehyde intermediate was formed, which prevents ring closure to patulin. Nevertheless, these data experimentally confirm that PatE is a *bona fide* patulin synthase by being able to produce patulin from ascladiol using dioxygen as electron acceptor.

Interestingly, PatE was also shown to oxidize 5-hydroxymethyl furfural (HMF), which is a highly attractive bio-based platform chemical [22]. The alcohol and aldehyde functional groups of HMF can undergo multiple oxidation and reduction reactions, thereby forming a variety of interesting products, including 2,5-diformylfuran (DFF), 5-formyl-2-furancarboxylic acid (FFCA) and 2,5-furandicarboxylic acid (FDCA) [22]. DFF is an attractive compound as it can be used as a building block for the synthesis of antifungal agents [23], ligands [24] and polymers [25,26]. FDCA is a highly sought-after building block for polymers [27]. Using HPLC, the conversion of HMF by PatE was monitored to determine what main products are obtained upon HMF oxidation. It was found that, after 72 h, most of the HMF was converted into DFF and FFCA while only trace amounts of FDCA were detected (Fig. 6A). In the first few hours of the reaction, exclusively DFF was produced (Fig. 6B). Hence, by using shorter reaction times and continuous feeding with HMF, it should be possible to obtain DFF in high purity making patulin synthase a potential candidate biocatalyst for DFF production strategies.

Structural properties of patulin synthase

According to size-exclusion chromatography and mass photometry, PatE is mainly a dimer in solution (Fig. 7 and Fig. S2). To have detailed insights into the molecular functioning of PatE, we set out to determine its crystal structure. Yellow cuboid crystals were obtained with 19.5% PEG6000 and 0.1 M sodium acetate that diffracted up to 2.4 Å. Elucidation of the crystal structure revealed an overall structure that is similar to other members of the GMC superfamily, including the
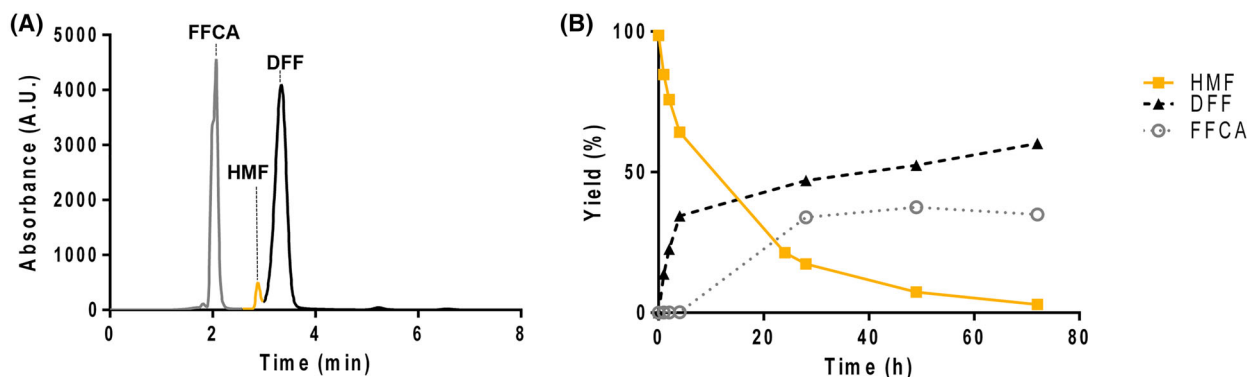

Fig. 6. (A) HPLC chromatogram from 10 μM PatE with 25 mM HMF in 100 mM KPi pH 7.5 after 72 h. (B) Conversion over time of 10 μM PatE with 25 mM HMF in 100 mM KPi pH 7.
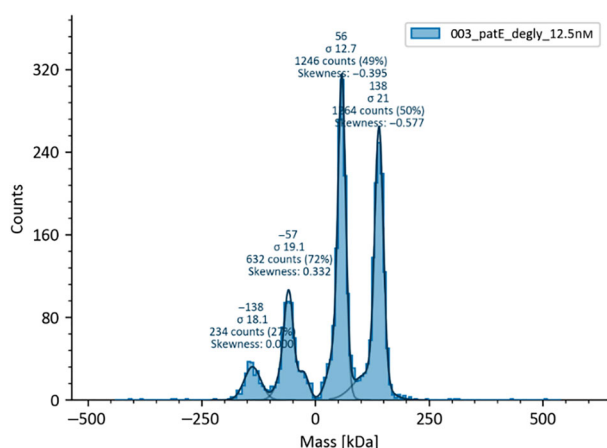
Fig. 7. Mass photometry of 12.5 ng deglycosylated PatE in 100 mM KPi pH 7.5.

well-known glucose oxidase and aryl-alcohol oxidase. GMC-type flavoproteins oxidases typically contain a conserved N-terminal FAD binding domain (F-domain), which has a sequence motif characteristic of the Rossmann fold [28]. In PatE, the F-domain is composed of residues starting from the N terminus to amino acid 368 (Fig. 8A, PDB: 8BXL). In contrast to the conserved F-domain, there is typically little sequence similarity of the substrate-binding domain (S-domain) displayed amongst GMC family members [17]. This can also be observed for patulin synthase, of which the S-domain is comprised of residues 369 till 620 and has very low sequence identities when compared to known GMC-type proteins. Structural alignment using PDBeFold revealed that patulin synthase is most comparable to the aryl-alcohol oxidase (AAO) from *Pleurotus eryngii* (PDB: 5OC1), with an RMSD value of 1.56 Å and 29% sequence identity (Fig. 8B) [29]. A prominent structural difference is that patulin synthase forms a dimer in solution, while AAO has been characterized as a monomer. Sequence alignment revealed that patulin synthase has an N-terminal extension comprising of 50 amino acids, out of which 22 are part of the signal peptide (Fig. S3). The other 28 N-terminal amino acids are located at the dimerization interface of patulin synthase (Fig. S4) and contribute to dimerization. Patulin synthase was predicted to have seven glycosylation sites, and five out of these seven sites were indeed decorated with an *N*-acetylglucosamine moiety. Furthermore, the crystal structure was found to contain one disulphide bridge, which is formed between residues Cys584 and Cys590.

A number of GMC family oxidases have been thoroughly studied concerning their catalytic mechanism. This has revealed that substrate oxidation involves a
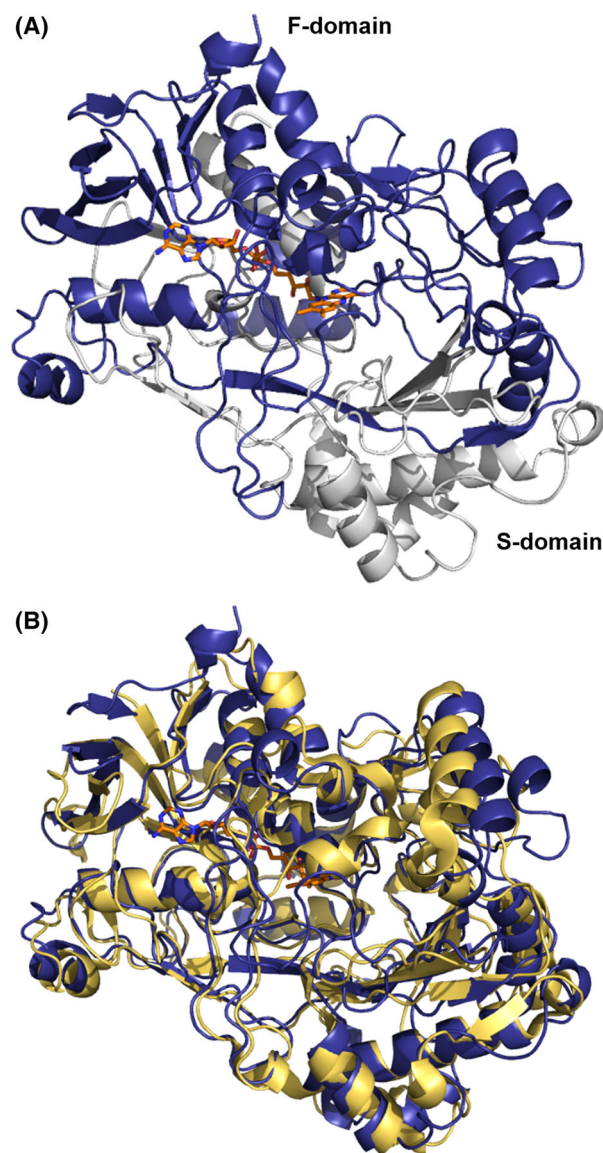
Fig. 8. (A) Monomeric structure of PatE. In deep blue the F-domain, in grey the S-domain and in orange the FAD cofactor is represented. The structures were visualized using the PyMOL Molecular Graphics System, Version 2.0, Schrodinger, LLC. (B) Structural alignment of PatE (deep blue, PDB: 8BXL) with the aryl-alcohol oxidase from *P. eryngii* (yellow, PDB: 5OC1). The structures were visualized using the PyMOL Molecular Graphics System, Version 2.0, Schrodinger, LLC.

proton abstraction step by a conserved catalytic histidine in the active site [30]. Next to the fully conserved histidine residue, the presence of a spatially conserved histidine residue has been found in multiple enzymes of the respective superfamily members [31]. Here, His526 and His570 are present in the active site, one of which is the corresponding catalytic base and the other the hydrogen bond donor. The strikingly narrow

Fig. 9. Active site of PatE with in light blue the substrate pocket connected to the FAD cofactor. The structure was visualized using PYMOL.

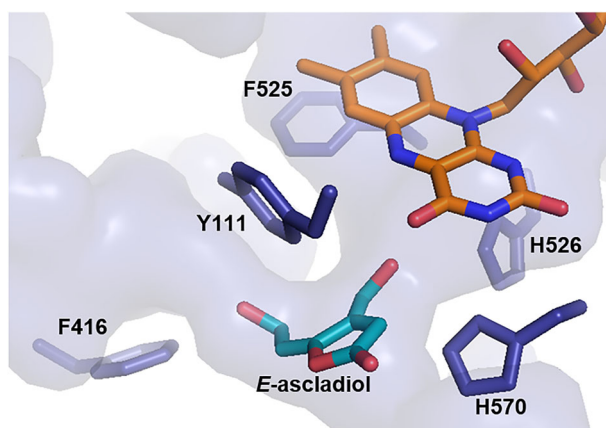active site is an interesting topological feature of patulin synthase (Fig. 9), which is a feature shared with the AAO from *P. eryngii*. There are comparable active site residues creating a narrow bottleneck essential for retaining the substrate in a catalytically active conformation (Fig. 10). In patulin synthase, these three residues correspond to Tyr111, Phe416 and Phe525. Tyr111 is situated above the FAD cofactor, and in AAO, it is closely involved in the stabilization of aromatic substrates via π–π interactions [32]. Phe525 is important in guiding the electron acceptor molecular

oxygen close to the flavin C4a [33]. The third residue, Phe416, is a residue that has been shown to regulate substrate-binding and product release in AAO [34]. Here, Phe416 could take up the same role and thereby influence the substrate acceptance scope by preferentially only allowing hydrophobic aromatic alcohols.

To confirm the potential role of the residues above, soaking experiments were performed with several PatE substrates. Unfortunately, none of the soaked crystals was found to be in complex with a ligand. Therefore, (*E*)-ascladiol was docked *in silico*. Fig. 10A shows a docked pose of the substrate in which (*E*)-ascladiol comfortably resides in the narrow substrate pocket. The binding orientation of ascladiol is very similar to the observed binding of a substrate analogue, *p*-anisic acid, in AAO (Fig. 10B). The hydroxymethyl functionality of the docked (*E*)-ascladiol is closely located to the flavin N5 atom and to the two histidine residues His526 and His570. Such orientation is in line with substrate deprotonation by one of the two histidines and hydride transfer of *p*-anisyl alcohol to the N5 atom of FAD in AAO. Residue Tyr111 is situated on the *Re*-face of the FAD cofactor and closely interacts with the furan ring of (*E*)-ascladiol in an edge-to-face conformation. This residue is essential for this type of π–π stacking interactions and therefore crucial in tuning the substrate acceptance scope. Moreover, the hydroxyl group of Tyr111 can have additional stabilizing interactions with the hydroxyethylidene functional group of (*E*)-ascladiol. Phe416 is lining the entrance of
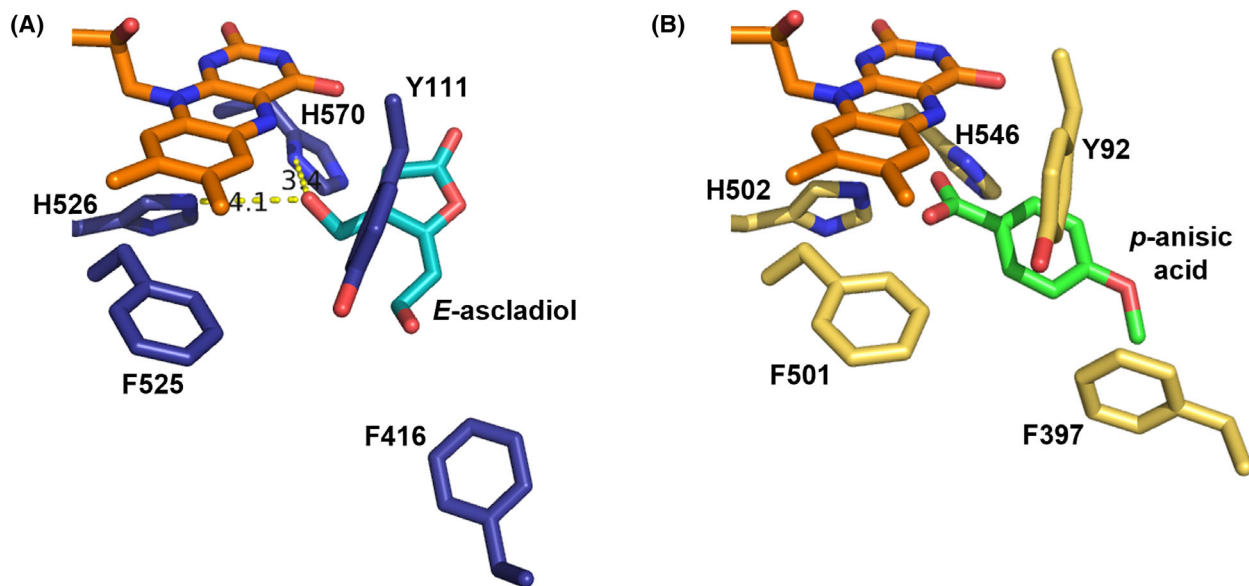

Fig. 10. (A) Docked binding pose of (*E*)-ascladiol (blue sticks) in the active site of PatE (deep blue). (B) Binding pose of *p*-anisic acid (green sticks) in the active site of aryl-alcohol oxidase from *P. eryngii* (yellow, PDB ID: 5OC1). The FAD cofactor is represented in orange in both figures, distances are expressed in angstroms, and the structures were visualized using PYMOL.

the substrate channel and therefore defines the entry of substrate and release of product. Patulin synthase encompasses a set of polar residues, namely Thr371, Ser372, Gln419, Tyr422 and Asp522, which are not found in AAO. Some of these residues may be involved in hydrogen bonding with the polar functional groups of (*E*)-ascladiol, thereby differentiating its activity with regard to AAO. Moreover, when compared with AAO, there are several loop regions that are more extended and covering the entrance of its active site. This may also contribute to tuning of substrate acceptance profile of PatE.

In conclusion, our study on patulin synthase, PatE, has shown that it is a GMC-type flavoenzyme that efficiently oxidizes the patulin precursor ascladiol to form patulin. It can use dioxygen as electron acceptor, thus acting as an oxidase. Patulin synthase also accepts other substrates and has a clear preference towards aromatic alcohols. These features are shared with fungal AAOs and are in line with the observation that the structure of PatE resembles the crystal structure of an AAO. The resemblance extends to the active site architecture where several substrate-binding pocket residues and catalytic residues are fully conserved amongst these fungal flavoprotein oxidases. Nonetheless, there are also clear structural differences that can explain that PatE is tuned for acting on ascladiol. The obtained insights and the availability of the recombinant enzyme may help to design strategies aimed at lowering the risk on formation of the mycotoxin. For example, development of PatE inhibitors could be explored. PatE may also develop as a useful biocatalyst for synthetic chemistry, for example for conversion of HMF. Our results also reveal that recombinant expression of PatE as secreted protein using an *Aspergillus* strain as host [20] is very effective, leading to relatively pure, fully flavinylated and active enzyme. It allows to produce His-tagged protein, enabling affinity purification. Such enzyme production platform is very attractive because expression of fungal enzymes in other hosts often leads to no or poor expression. For example, AAOs are notoriously difficult to express in *E. coli* [35], often leading to the formation of inclusion bodies. The newly developed expression system is a promising new tool for future studies on other fungal flavoproteins or other interesting protein targets that are troublesome to obtain using other expression systems.

Materials and methods

Reagents

Ni-Sepharose 6 Fast Flow was from Cytiva (Marlborough, MA, USA), 4-aminoantipyrine was from Acros Organics (Geel, Belgium), dichloro-2-hydroxybenzenesulfonic acid from Alfa-Aesar (Tewksbury, MA, USA), L-arabinose was from Biosynth (Compton, UK), and all other chemicals were from Sigma-Aldrich (Burlington, MA, USA). (*Z*)-Ascladiol was synthesized as described in the Supporting Information.

Cloning, transformation and expression of PatE in *Aspergillus niger*

For establishing the expression of His-tagged PatE (with a C-terminal His6-tag), a newly developed expression procedure that involves the use of CRISPR/Cas9 was exploited [20]. By multiple and targeted chromosomal integrations of the gene in *Aspergillus niger*, high-level expression was obtained [20]. The original *P. expansum* signal sequence was used for expression in *A. niger*. Cultures were prepared by inoculating a 300 mL Erlenmeyer flask containing 100 mL of complete medium (CM) with freshly harvested spores (1×10^8 spores). Cultures were grown at 4 ***g*** at 30 °C up to 4 days. Full details on plasmid construction, transformation and cultivation can be found in [20].

Protein purification

Purification was performed by concentrating the cleared medium using an Amicon-ultra® 15 centrifugal filter unit (10 kDa cut-off). The concentrated sample was incubated for 30 min with pre-equilibrated Ni-Sepharose resin with buffer A (100 mM KPi, 150 mM NaCl, pH 7) at 4 °C. Thereafter, the nonbinding proteins were eluted by washing with 5 column volumes (CV) of buffer A and 3 CV of buffer B (100 mM KPi, 150 mM NaCl, 20 mM imidazole, pH 7). The protein of interest was eluted with 1.5 CV of buffer C (100 mM KPi, 150 mM NaCl, 500 mM imidazole, pH 7). Desalting was performed by exchanging the buffer with buffer A using an Amicon-ultra® 15 centrifugal filter unit (10 kDa cut-off). The concentration of PatE was determined by measuring absorbance at 463 nm and using an extinction coefficient of $\varepsilon_{463} = 9.7$ mM^{-1}·cm^{-1}. The extinction coefficient was determined using a stock solution of FAD according to the method described in [36].

Thermal stability

*Thermo*FAD was employed as method to assess the thermostability of the enzyme, which monitors fluorescence of the flavin cofactor during thermal unfolding [37]. For this assay, 20 μM PatE was prepared in buffers with varying pH values. A 100 mM citrate buffer was used for pH values between 5 and 6.5, a 100 mM KPi buffer for pH values between 6.5 and 8, and a 100 mM TRIS buffer for pH values between 8 and 9. The measurements were performed in duplicate. An RT-PCR thermocycler (CFX96 Bio-Rad) was used and fluorescence was examined in a temperature range of 25–95 °C with 0.5 °C·min^{-1} increment.

pH optimum for activity

For determining the pH optimum for enzyme activity, the rate of oxygen consumption was measured using an Oxygraph Plus (Hansatech Instruments Ltd., Pentney, UK). Reactions were performed with 1 μM enzyme, 10 mM 3-methoxybenzyl alcohol and various buffers with different pH values, in a final volume of 1 mL. A 100 mM citrate buffer was used for pH values between 5 and 6.5, a 100 mM KPi buffer for pH values between 6.5 and 8, and a 100 mM TRIS buffer for pH values between 8 and 9. Rates were derived from the initial linear slope of the oxygen depletion curves.

Steady-state kinetics

An established horseradish peroxidase (HRP)-coupled oxidase assay was used to measure oxidase activity of the enzyme [38]. Upon substrate oxidation, H_2O_2 is formed and used by HRP to convert 4-aminoantipyrine and dichloro-2-hydroxybenzenesulfonic acid into a coloured product. Change in absorbance at 515 nm ($\varepsilon_{515} = 26$ cm^{-1}·mM^{-1}) was measured to derive the rate towards a multitude of substrates. To obtain steady-state kinetic parameters, the assay was performed with various substrate concentrations and 1 μM of enzyme in 100 mM KPi pH 7.5 buffer. GRAPHPAD PRISM (v6.05 for Windows, La Jolla, CA, USA) was used to process the rates and fitted using the Michaelis–Menten formula ($Y = k_{cat}*X/(K_M + X)$) to obtain the K_M and k_{cat}. When needed, data were fitted with a more elaborate formula that includes substrate inhibition (K_I): $Y = k_{cat}*X/(K_M + X*(1 + X/K_I))$, from [39].

Chemical analyses of conversions

The conversion of ascladiol was analysed using high-performance liquid chromatography (HPLC) on a Jasco LC-Net II/ADC equipped with a C18 Gemini® column (110 Å, 5 μm, 250 × 4.6 mm) and a precolumn of the same material. The mobile phase consisted of 95 : 5 MQ/ACN, flow rate of 0.7 mL·min^{-1} and detection at 276 nm. The reactions were set up in duplicate using 0.5 mM of ascladiol, 0.1 μM patulin synthase in 100 mM KPi pH 7.5 and incubated at 25 °C at 4 *g* for 2 h. Time-point samples were taken and diluted 10 times in a 50 : 50 MQ/ACN solution. The samples were spun down (1 min, 18 000 *g*), and the supernatant was analysed.

The conversion of HMF was analysed with a Jasco LC-Net II/ADC equipped with a XSelect CSH Fluoro-Phenyl column (130 Å, 5 μm, 4.6 × 250 mm), and precolumn of the same material. The mobile phase consisted of 12 mM KPi at pH 7 and ACN, with a flow rate of 1.2 mL·min^{-1} and detection at 268 nm. The KPi/ACN ratio decreased from 75 : 25 to 40 : 60 in 6 min, which was held stable for 0.5 min, after which it increased to 75 : 25 in 1.5 min. This

ratio was maintained for 2 min, making up a total of 10 min. The reactions were set up in duplicate using 25 mM HMF and 10 μM patulin synthase in 100 mM KPi pH 7.5 and incubated at 25 °C at 4 *g* for 72 h. Time-point samples were taken and diluted five times in a 50 : 50 12 mM KPi pH 7/ACN solution. The supernatant was taken for analysis.

Protein crystallization and structure elucidation

Purified recombinant patulin synthase contained several *N*-glycosylation sites. For crystallization experiments, the asparagine-linked glycosyl moieties were cleaved off using EndoH leaving behind one *N*-acetylglucosamine (GlcNAc) moiety. The enzyme was further purified by size-exclusion chromatography using a Superdex200 10/300 column (Cytiva) with an Äkta purifier. Protein elution was monitored using two wavelengths (280 and 463 nm). The fractions with the most absorbance at 463 nm were pooled and concentrated using Amicon-ultra® 4 (10 kDa cut-off filter) to a final concentration of 6.9 mg·mL^{-1}. Initial crystallization conditions were screened using different screenings with a Mosquito crystallization robot (TTP LabTechs, Melbourn, UK). Large yellow cuboid crystals were obtained under different conditions (Fig. S10). After optimization, the best condition was 0.2 M $CaCl_2$, 19.5% PEG6000 and 0.1 M sodium acetate pH 5 using the sitting drop vapour diffusion method. As a cryoprotectant, 25% glycerol was used and crystals were flash-frozen in liquid nitrogen and sent to ESRF for data collection. The best crystal diffracted at 2.4 Å resolution using the MASSIF-1 beamline [40]. Data were scaled using IMOSFLM of the CCP4 package [41]. PHENIX was used for molecular replacement [42]. COOT [27] and REFMAC5 [43], both part of the CCP4 package, were

Table 2. Crystal and X-ray diffraction data of patulin synthase.

PDB entry	8BXL
Space group	$P12_11$
Unit cell axes (Å)	104.84, 144.16, 155.24
Unit cell angles (deg)	90, 91.53, 90
Resolution (Å)	48.69 (2.44)
R_{merge} (%)	14.8 (106.5)
R_{pim} (%)	9.4 (6.95)
$CC_{1/2}$	0.978 (0.720)
Completeness (%)	99.8 (99.7)
No. of unique reflections	179 872 (8892)
Multiplicity	3.5 (3.4)
Overall $I/\sigma(I)$	9.5 (3.0)
No. of protein residues	3540
No. of FAD molecules	6
No. of water molecules	1992
R/R_{free}	18.2/22.2
RMSD for bond lengths (Å)	0.0182
RMSD for bond angles (Å)	1.44
Ramachandran outliers (%)	1.39

employed for structural refinement. Details of the collected data set are summarized in Table 2.

Acknowledgements

Conflict of interest

The authors declare no conflict of interest.

Author contributions

GT wrote the paper and performed the experiments. AB and HR assisted with X-ray crystallography experiments. IM synthesized ascladiol. JV, MA and AFJR produced patulin synthase in *Aspergillus niger*. AM and MWF assisted with writing the paper. All authors reviewed the paper.

Peer review

The peer review history for this article is available at https://www.webofscience.com/api/gateway/wos/peer-review/10.1111/febs.16804.

Data availability statement

Structural data are openly available in the wwPDB under the accession number 8BXL. Additional data supporting the results of this study can be found in the Supporting Information or are available from the corresponding authors upon reasonable request.

References

1 Demirel R, Sariozlu NY & Semra İ (2013) Polymerase chain reaction (PCR) Terverticillate *Penicillium* species agricultural soils in Eskişehir Province. *Brazilian Arch Biol Technol* **56**, 980–984.

2 Gutarowska B, Kosmowska M, Wiszniewska M, Pałczyński C & Walusiak-Skorupa J (2012) An investigation of allergenic proteins produced by moulds on building materials. *Indoor Built Environ* **21**, 253–263.

3 Li B, Chen Y, Zong Y, Shang Y, Zhang Z, Xu X, Wang X, Long M & Tian S (2019) Dissection of patulin biosynthesis, spatial control and regulation mechanism in *Penicillium expansum*. *Environ Microbiol* **21**, 1124–1139.

4 Puel O, Galtier P & Oswald IP (2010) Biosynthesis and toxicological effects of Patulin. *Toxins (Basel)* **2**, 613–631.

5 Moake MM, Padilla-Zakour OI & Worobo RW (2005) Comprehensive review of Patulin control methods in foods. *Compr Rev Food Sci Food Saf* **4**, 8–21.

6 Vidal A, Ouhibi S, Ghali R, Hedhili A, De Saeger S & De Boevre M (2019) The mycotoxin patulin: an updated short review on occurrence, toxicity and analytical challenges. *Food Chem Toxicol* **129**, 249–256.

7 Saleh I & Goktepe I (2019) The characteristics, occurrence, and toxicological effects of patulin. *Food Chem Toxicol* **129**, 301–311.

8 Morales H, Marín S, Ramos AJ & Sanchis V (2010) Influence of post-harvest technologies applied during cold storage of apples in *Penicillium expansum* growth and patulin accumulation: a review. *Food Control* **21**, 953–962.

9 Tannous J, Keller NP, Atoui A, El Khoury A, Lteif R, Oswald IP & Puel O (2018) Secondary metabolism in *Penicillium expansum*: emphasis on recent advances in patulin research. *Crit Rev Food Sci Nutr* **58**, 2082–2098.

10 Varga J, Rigó K, Tóth B, Téren J & Kozakiewicz Z (2003) Evolutionary relationships among *Aspergillus* species producing economically important mycotoxins. *Food Technol Biotechnol* **41**, 29–36.

11 Dombrink-Kurtzman MA & Engberg AE (2006) *Byssochlamys nivea* with patulin-producing capability has an isoepoxydon dehydrogenase gene (idh) with sequence homology to *Penicillium expansum* and *P. griseofulvum*. *Mycol Res* **110**, 1111–1118.

12 Samson RA, Houbraken J, Varga J & Frisvad JC (2009) Polyphasic taxonomy of the heat resistant ascomycete genus *Byssochlamys* and its *Paecilomyces* anamorphs. *Persoonia* **22**, 14–27.

13 Houbraken J, Samson RA & Frisvad JC (2005) *Byssochlamys*: significance of heat resistance and mycotoxin production. *Adv Exp Med Biol* **571**, 211–224.

14 Frisvad JC, Smedsgaard J, Larsen TO & Samson RA (2004) Mycotoxins, drugs and other extrolites produced by species in *Penicillium* subgenus *Penicillium*. *Stud Mycol* **2004**, 201–241.

15 Dijkman WP, De Gonzalo G, Mattevi A & Fraaije MW (2013) Flavoprotein oxidases: classification and applications. *Appl Microbiol Biotechnol* **97**, 5177–5188.

16 Fraaije MW & Mattevi A (2000) Flavoenzymes: diverse catalysts with recurrent features. *Trends Biochem Sci* **25**, 126–132.

17 Sützl L, Foley G, Gillam EMJ, Bodén M & Haltrich D (2019) The GMC superfamily of oxidoreductases revisited: analysis and evolution of fungal GMC oxidoreductases. *Biotechnol Biofuels* **12**, 1–18.

18 Nguyen QT, Romero E, Dijkman WP, De Vasconcellos SP, Binda C, Mattevi A & Fraaije MW (2018) Structure-based engineering of *Phanerochaete chrysosporium* alcohol oxidase for enhanced oxidative power toward glycerol. *Biochemistry* **57**, 6209–6218.

19 Dijkman WP & Fraaije MW (2014) Discovery and characterization of a 5-hydroxymethylfurfural oxidase from *Methylovorus* sp. strain MP688. *Appl Environ Microbiol* **80**, 1082–1090.

20 Arentshorst M, Valappil PK, Mózsik L, Regensburg-Tuïnk TJG, Seekles S, Tjallinks G, Fraaije MW, Visser J & Ram AFJ (2023) A CRISPR/Cas9-based multicopy integration system for protein production in *Aspergillus niger*. *FEBS J* **290**, 5127–5140.

21 Lykakis IN, Zaravinos IP, Raptis C & Stratakis M (2009) Divergent synthesis of the co-isolated mycotoxins longianone, isopatulin, and (*Z*)-ascladiol via furan oxidation. *J Org Chem* **74**, 6339–6342.

22 Martin C, Ovalle Maqueo A, Wijma HJ & Fraaije MW (2018) Creating a more robust 5-hydroxymethylfurfural oxidase by combining computational predictions with a novel effective library design. *Biotechnol Biofuels* **11**, 1–9.

23 Del Poeta M, Schell WA, Dykstra CC, Jones S, Tidwell RR, Czarny A, Bajic M, Bajic M, Kumar A, Boykin D *et al.* (1998) Structure-In vitro activity relationships of Pentamidine analogues and Dication-substituted Bis-Benzimidazoles as new antifungal agents. *Antimicrob Agents Chemother* **42**, 2495–2502.

24 Richter DT & Lash TD (1999) Oxidation with dilute aqueous ferric chloride solutions greatly improves yields in the "4+1" synthesis of sapphyrins. *Tetrahedron Lett* **40**, 6735–6738.

25 Xiang T, Liu X, Yi P, Guo M, Chen Y, Wesdemiotis C, Xu J & Pang Y (2013) Schiff base polymers derived from 2,5-diformylfuran. *Polym Int* **62**, 1517–1523.

26 Amarasekara AS, Green D & McMillan E (2008) Efficient oxidation of 5-hydroxymethylfurfural to 2,5-diformylfuran using Mn(III)-salen catalysts. *Catal Commun* **9**, 286–288.

27 Emsley P & Cowtan K (2004) *Coot*: model-building tools for molecular graphics. *Acta Crystallogr D* **60**, 2126–2132.

28 Kiess M, Hecht H-J & Kalisz HM (1998) Glucose oxidase from *Penicillium amagasakiense*. *Eur J Biochem* **252**, 90–99.

29 Carro J, Martínez-Júlvez M, Medina M, Martínez AT & Ferreira P (2017) Protein dynamics promote hydride tunnelling in substrate oxidation by aryl-alcohol oxidase. *Phys Chem Chem Phys* **19**, 28666–28675.

30 Gadda G (2008) Hydride transfer made easy in the reaction of alcohol oxidation catalyzed by flavin-dependent oxidases. *Biochemistry* **47**, 13745–13753.

31 Wongnate T & Chaiyen P (2013) The substrate oxidation mechanism of pyranose 2-oxidase and other related enzymes in the glucose-methanol-choline superfamily. *FEBS J* **280**, 3009–3027.

32 Ferreira P, Hernández-Ortega A, Lucas F, Carro J, Herguedas B, Borrelli KW, Guallar V, Martínez AT & Medina M (2015) Aromatic stacking interactions govern catalysis in aryl-alcohol oxidase. *FEBS J* **282**, 3091–3106.

33 Hernández-Ortega A, Lucas F, Ferreira P, Medina M, Guallar V & Martínez AT (2011) Modulating O₂ reactivity in a fungal flavoenzyme: involvement of aryl-alcohol oxidase Phe-501 contiguous to catalytic histidine. *J Biol Chem* **286**, 41105–41114.

34 Carro J, Amengual-Rigo P, Sancho F, Medina M, Guallar V, Ferreira P & Martínez AT (2018) Multiple implications of an active site phenylalanine in the catalysis of aryl-alcohol oxidase. *Sci Rep* **8**, 1–12.

35 Ruiz-Dueñas FJ, Ferreira P, Martínez MJ & Martínez AT (2006) In vitro activation, purification, and characterization of *Escherichia coli* expressed aryl-alcohol oxidase, a unique H₂O₂-producing enzyme. *Protein Expr Purif* **45**, 191–199.

36 Peter Macheroux (1999) UV-visible spectroscopy as a tool to study flavoproteins. *Methods Mol Biol* **131**, 1–7.

37 Forneris F, Orru R, Bonivento D, Chiarelli LR & Mattevi A (2009) *ThermoFAD, a Thermofluor®-adapted flavin ad hoc detection system for protein folding and ligand binding. *FEBS J* **276**, 2833–2840.

38 Vojinović V, Azevedo AM, Martins VCB, Cabral JMS, Gibson TD & Fonseca LP (2004) Assay of H₂O₂ by HRP catalysed co-oxidation of phenol-4-sulphonic acid and 4-aminoantipyrine: characterisation and optimisation. *J Mol Catal B Enzym* **28**, 129–135.

39 Copeland RA (2000) Enzymes: A Practical Introduction to Structure, Mechanism, and Data Analysis. Wiley, Hoboken, NJ.

40 Bowler MW, Nurizzo D, Barrett R, Beteva A, Bodin M, Caserotto H, Delagenière S, Dobias F, Flot D, Giraud T *et al.* (2015) *MASSIF*-1: a beamline dedicated to the fully automatic characterization and data collection from crystals of biological macromolecules. *J Synchrotron Radiat* **22**, 1540–1547.

41 Battye TGG, Kontogiannis L, Johnson O, Powell HR & Leslie AGW (2011) *iMOSFLM*: a new graphical interface for diffraction-image processing with *MOSFLM*. *Acta Crystallogr D* **67**, 271–281.

42 McCoy AJ, Grosse-Kunstleve RW, Adams PD, Winn MD, Storoni LC & Read RJ (2007) *Phaser* crystallographic software. *J Appl Cryst* **40**, 658–674.

43 Kovalevskiy O, Nicholls RA, Long F, Carlon A & Murshudov GN (2018) Overview of refinement procedures within *REFMAC* 5: utilizing data from different sources. *Acta Crystallogr D* **74**, 215–227.

Supporting information

Additional supporting information may be found online in the Supporting Information section at the end of the article.

Fig. S1. HPLC profiles during different time intervals of the biocatalytic reaction with 0.5 mM of ascladiol and 0.1 μM PatE.

Fig. S2. Size-exclusion chromatography profile of PatE using a Superdex 200 10/300 column with 50 mM HEPES, 30 mM NaCl pH 7.

Fig. S3. Sequence alignment of patulin synthase (PatE, PDB: 8BXL, AIG62134.1, NCBI) with the aryl-alcohol oxidase from *Pleurotus eryngii* (AAO, PDB: 5OC1, AAC72747.1, NCBI).

Fig. S4. Dimerization interface of PatE with in green the N-terminal extension.

Fig. S5. Crystals of PatE obtained with screening condition 0.2 M CaCl$_2$, 0.1 M NaOAc pH 5, 19.5% PEG6000.

Fig. S6. ^{1}H NMR (top) and ^{13}C (bottom) spectra of methyl 3-methoxycarbonyl-2-furylacetate (2).

Fig. S7. ^{1}H NMR (top) and ^{13}C (bottom) spectra of 3-hydroxymethyl-2-furylethanol (3).

Fig. S8. ^{1}H NMR (top) and ^{13}C (bottom) spectra of (2-(2-acetoxyethyl)furan-3-yl)methyl acetate (4).

Fig. S9. ^{1}H NMR (top) and ^{13}C (bottom) spectra of (2-(2-acetoxyethyl)-2-hydroxy-5-oxo-2,5-dihydrofuran-3-yl)methyl acetate (5).

Fig. S10. ^{1}H NMR (top) and ^{13}C (bottom) spectra of (*Z*)-ascladiol diacetate (6).

Fig. S11. ^{1}H NMR (top) and ^{13}C (bottom) spectra of (*Z*)-ascladiol (7).

Table S1. Substrates tested for activity using the HRP-based assay.

Scheme S1. Synthetic route for synthesizing (*Z*)-Ascladiol from acetone dicarboxylic acid dimethyl ester.